Solar Energetic Particles

Donald V. Reames
NASA/Goddard Space Flight Center, Greenbelt, MD 20771, U.S.A.

1. Introduction

Solar energetic particle (SEP) events are responsible for some of the highest particle intensities that we have seen in space near Earth. The solar wind, which blows continuously at speeds of 300-800 km/s, corresponds to proton energies of 0.5 to 3 keV. Protons in SEP events have energy spectra that span the range from ~10 keV to ~10 GeV. The events can have very rapid onsets and have durations that range from a few hours to several days [34].

There are 2 distinct classes of SEP events corresponding to 2 physical mechanisms of particle acceleration. The event classes are called "impulsive" and "gradual" for historical reasons, although they roughly reflect differences in the time scales of the SEP events and the associated solar flares (see reviews by Gosling [10], Kahler [11, 13], Reames [32, 33, 34], and Tylka [47]):

(A) Particles in "impulsive" SEP events have 1000-fold enhancements in the isotopic ratio ^{3}He/^{4}He, compared with normal coronal abundances. These ^{3}He-rich events have $0.1 \leq {}^3\text{He}/{}^4\text{He} \leq 10$. They also have a progressive enhancement of heavy elements, relative to coronal abundances, that vary from a factor of ~10 for Fe/O to a factor of ~1000 for (Z≥50)/O. The unusual abundances are the result of resonant wave-particle interactions in turbulent regions of magnetic reconnection associated with solar flares. Impulsive SEP events are also electron-rich and are associated with type III radio bursts and small-to-moderate X-ray flares. Elements up through Si are fully ionized in these events and Fe of charge ~20 is seen, indicating that the ions come from a hot plasma with a temperature of $>10^7$ Kelvin (>10 MK). These events come from a small interval of solar longitude where the particles can follow magnetic field lines from the flare to the observer.

(B) Particles in "gradual" SEP events are accelerated at shock waves driven out from the Sun by fast coronal mass ejections (CMEs). The largest events can span more than 200^o in solar longitude since the shocks can easily cross magnetic field lines, accelerating particles as they go. The events can last for several days. Average element abundances and ionization states are usually similar to those in the ambient (~1-2 MK) corona and solar wind, although we will see that interesting variations do occur.

Figure 1 compares intensity-time profiles for a series of impulsive and gradual SEP events on the same time scale. As is clear from the figure, the largest and most energetic SEP events are all gradual events.

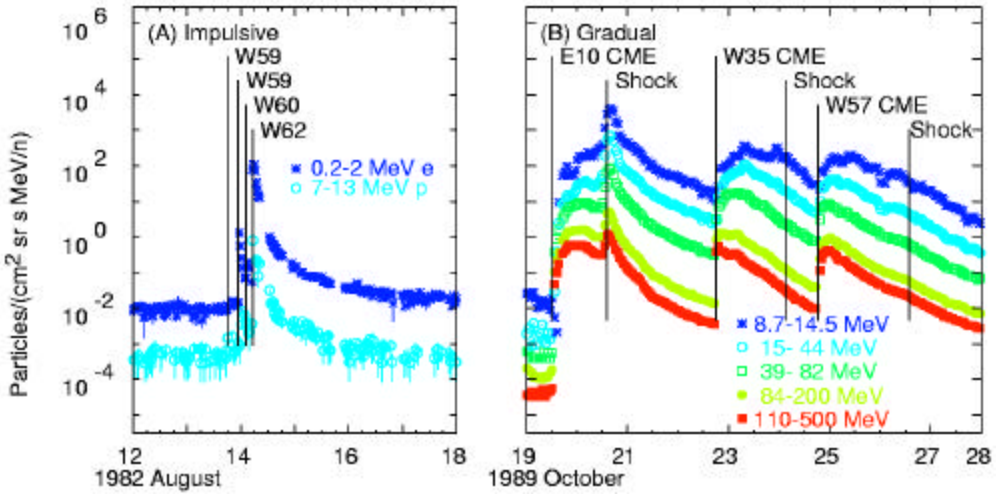

Figure 1. Various particle intensities are shown as a function of time for: (A) flare-associated impulsive SEP events, and (B) gradual SEP events associated with CME-driven shock waves.

The solar longitude distributions of gradual and impulsive events are compared in Figure 2. SEPs follow magnetic field lines from their source to the observer. Impulsive events are only seen when they come from flares near the footpoint of the spiral magnetic field line. The shock waves that produce gradual span a huge volume. These events are often seen associated with CMEs from behind the east and west limbs of the Sun as far as E120 and W140, however, these are omitted from the figure because their longitudes are less certain. CME-driven shock waves can expand in both longitude and latitude, over a very large volume.

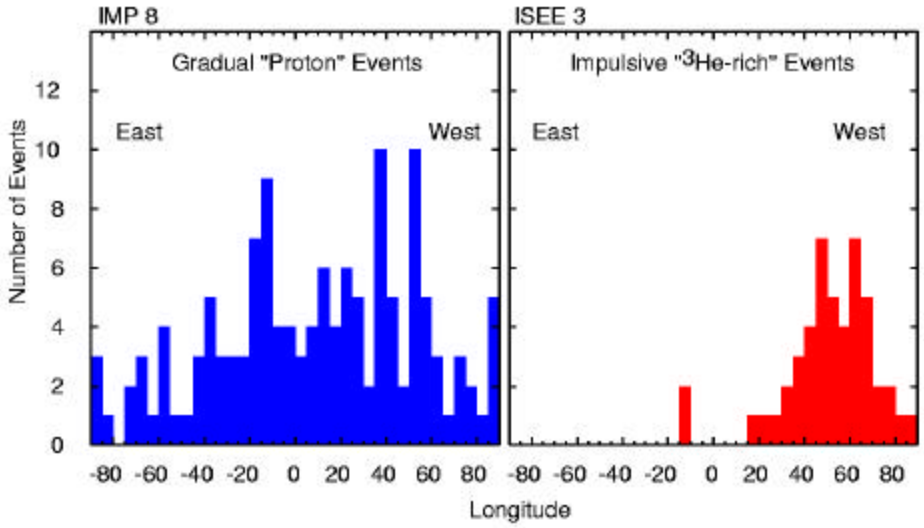

Figure 2. Distributions of solar source longitudes are shown for gradual and impulsive SEP events. Sources of gradual events are expanding CME-driven shock waves. Sources for impulsive events are point-like flares.

Ionization states of SEPs can be a powerful measure of the temperature of the source plasma where the ions are accelerated. Luhn *et al.* [22] showed that the average charge state of energetic Fe was Q_{Fe}=20.5 ± 1.2 in impulsive SEP events, indicating a hot source plasma of 10-20 MK (see Figure 3). Elements up through Si were fully ionized in impulsive events. For gradual events, Q_{Fe}=14.1 ± 0.2, slightly higher than that for Fe in the solar wind. Even for 200-600 MeV/amu Fe, Tylka *et al.* [48] found Q_{Fe}=14.2 ± 1.2 in the large gradual events of 1989.

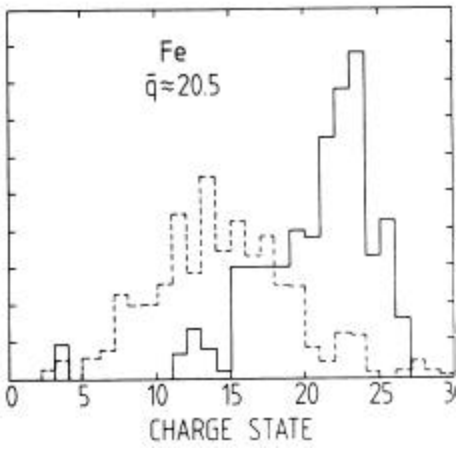

Figure 3. The distribution of ionization states of Fe in impulsive SEP events (solid) is compared with that in gradual (dashed) events (after Luhn *et al.* [22]).

However, ionization states alone may not distinguish gradual events since shock waves may begin sufficiently low in the corona where densities cause SEPs to be stripped during acceleration (Reames *et al.* [40]). In addition, shocks may accelerate residual suprathermal ions left over from impulsive events (Mason *et al.* [24]; Desai *et al.* [4]; Tylka *et al.* [50]).

2. Impulsive SEP Events

Impulsive SEP events were first distinguished by their unique isotopic and element abundances, indicating the presence of a unique acceleration mechanism. Figure 4 shows an impulsive SEP event with ^{3}He/^{4}He~10, when corrected for preexisting ^{4}He background. The corresponding ratio in the solar atmosphere and solar wind is ~0.0005. These large enhancements are now understood in terms of resonant wave-particle interactions in the flare plasma (see Fisk [6]; Temerin and Roth [46]; Roth and Temerin [44]). In recent models, beams of electrons streaming down the magnetic field lines generate electromagnetic ion-cyclotron waves at frequencies between the gyrofrequencies of H and ^{4}He, the two dominant ions in the plasma. The only species with a gy-

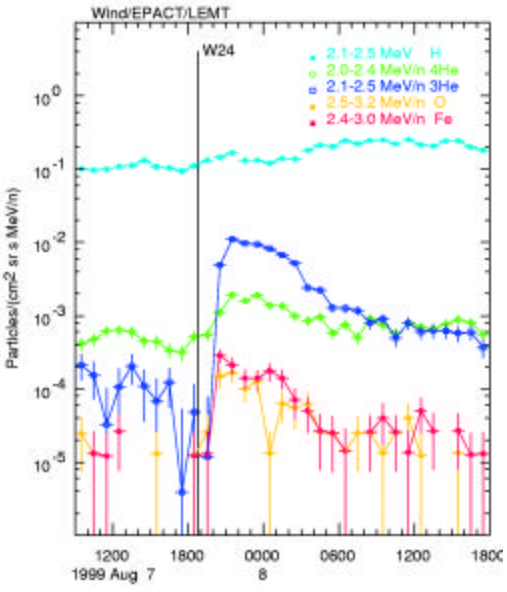

Figure 4. Intensities of various species are shown as a function of time in an impulsive SEP event.

rofrequency in that region is the rare isotope ^{3}He. Thus, ^{3}He is preferentially accelerated as it absorbs energy from the waves.

Fe is also enhanced relative to O in the event in Figure 4. In this event Fe/O~1, while the corresponding ratio in the solar corona is 0.13. Recently it has been possible to extend measurements of abundances in impulsive SEP events [37] to elements throughout the periodic table [35] as shown in Figure 5. While the enhancements in (Z>50)/O and ^{3}He/^{4}He can be very large in these events, event-to-event variations in the abundances, relative to the mean, are also large and are poorly correlated with each other.

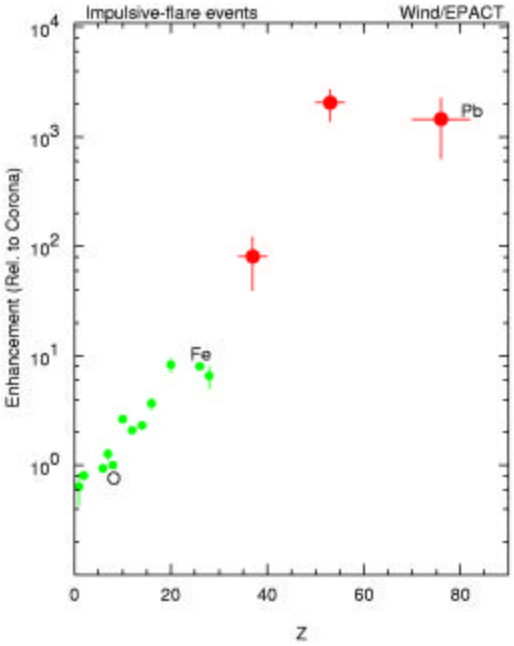

Figure 5. Element abundance enhancements at high Z can be very large for impulsive SEP events [35].

3. Gradual SEP Events

Gradual SEP events are the most intense events that we see, with the highest energy particles. Large events occur at the rate of ~20/yr. Because of their high intensities and long durations, large events are the easiest to measure and have been studied most completely.

3.1 Shock Acceleration and Shock Peaks

The highest intensities of <1 GeV protons that we see near Earth occur at intensity peaks at the time of shock passage. The SEP event of 1972 August 4 is one of the largest events seen since measurements in space have been available. Figure 6 compares fluxes in this event with those in other events. Unfortunately, the energy coverage of the Explorer 41

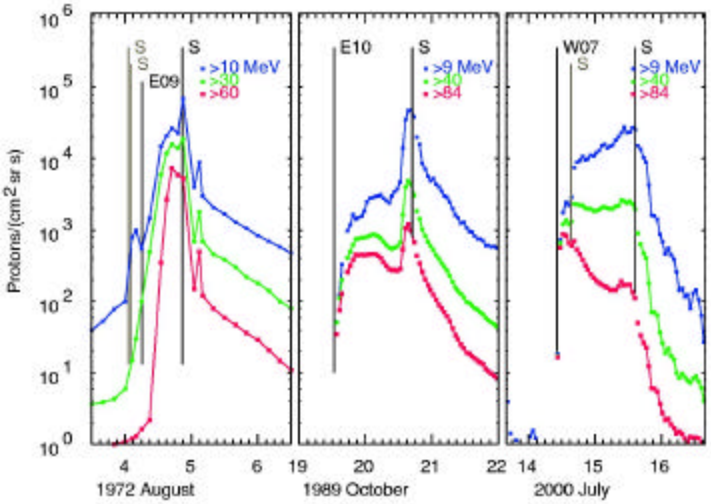

Figure 6. Proton flux peaks at the shocks are compared in historic and modern examples of gradual SEP events.

instrument does not extend to higher energies, nor do the intervals correspond well with the GOES measurements in the later events. However, peak fluxes of >60 MeV protons at the shock in the 1972 August 4 event even exceed the peaks of the >40 MeV protons in the later events.

Particles are accelerated at shocks when they resonantly scatter back and forth against Alfvén waves upstream and downstream of the shock. The particles gain an increment of velocity each transit of the shock (see Jones and Ellison [8]). As the particles stream away from the shock, they amplify Alfvén waves with wave vector $k=B/\mu P$, where B is the magnetic field strength, P is the particle rigidity or momentum per unit charge, and μ is the cosine of the particle pitch angle with respect to the magnetic field. As wave intensities increase, the particles are more efficiently trapped near the shock; hence, they gain more energy and then amplify resonant waves at this higher energy. Thus, the acceleration proceeds to higher and higher energies. Most of the waves are generated by protons, the most abundant species, while the other species act as test particles, probing the spectrum of the proton-generated waves. An equilibrium theory of acceleration by self-generated waves was developed for galactic cosmic rays by Bell [1] and was applied to solar and interplanetary shocks by Lee [18, 19]. Time-dependent particle transport and acceleration have been modeled by Ng *et al.* [30] and by Zank *et al.* [52].

As shocks move outward from the Sun they weaken, and the SEP energy spectra become steeper. However, Figure 7 shows that protons with energies up to 510-700 MeV can still peak at a shock that is driven by a fast CME coming from the region near central meridian on the Sun, such as the event of 2001 November 4. The event of 1989 October 19, shown at lower energies in Figure 6, also has a strong shock peak above 500 MeV.

Kahler *et al.* [17] found that the speed of a CME is one of the most important parameters in determining the peak proton intensity, wherever the peak occurred during an event. Figure 8 shows a recent study of this correlation.

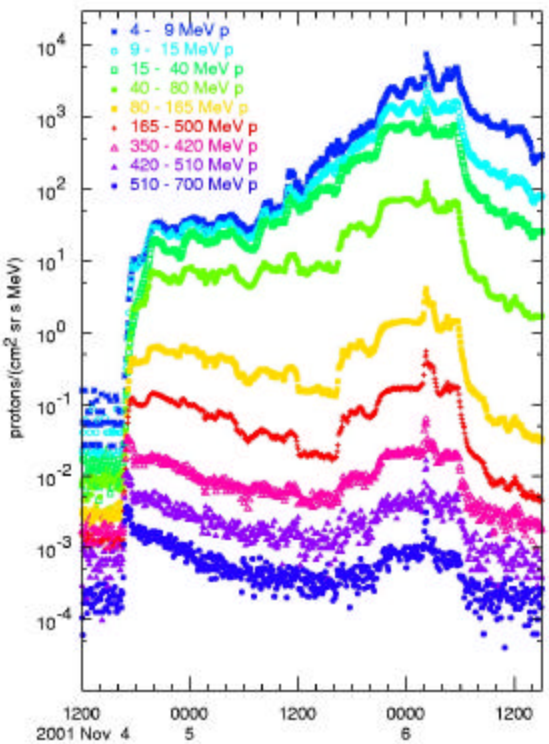

Figure 7. The peak at the time of shock passage is clearly defined early on November 6, even at proton energies as high as 510-700 MeV.

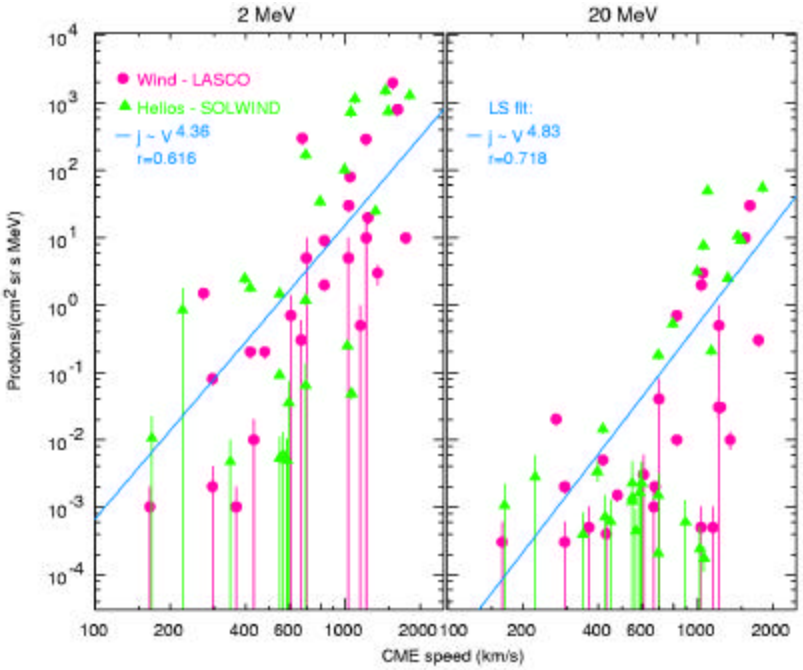

Figure 8. The correlation between peak proton intensities and CME speeds is shown for two particle energies for events on two combinations of spacecraft.

Kahler [13] realized that spectral variation affects the correlation with CME speed. Even with a perfect correlation at 2 MeV, differences in spectral slope would cause a large spread at 20 MeV. The longitude and angular spread of a CME also affect the probability that the shock intercepts the observer's flux tube.

Of course, CME observations were not available for the 1972 August 4 event. However, the average speed of the shock, from the Sun to Earth, in this event was 2900 km/s. This is far above the speed scale in Figure 8.

3.2 Spatial Distributions

The interplanetary magnetic field, carried outward by the ~400 km/s solar wind, is drawn into the well-known Parker spiral pattern by the rotation of the Sun. CMEs that move radially outward through the solar wind at high speed drive a bow shock where SEPs are accelerated. The spiral magnetic fields guide the particles in an asymmetric pattern as they flow away from the shock. Therefore, the shape of the particles intensity-time profile differs greatly depending upon the solar longitude of the CME source relative to that of an observer.

Figure 9 shows intensity-time profiles seen by observers at three different longitudes relative to the CME, which is assumed to be moving downward in the figure. The highest shock speed, hence the highest particle intensity, is expected to occur at the shock "nose." SEP intensities decrease as one moves along the shock front from the nose around to the flanks on either side.

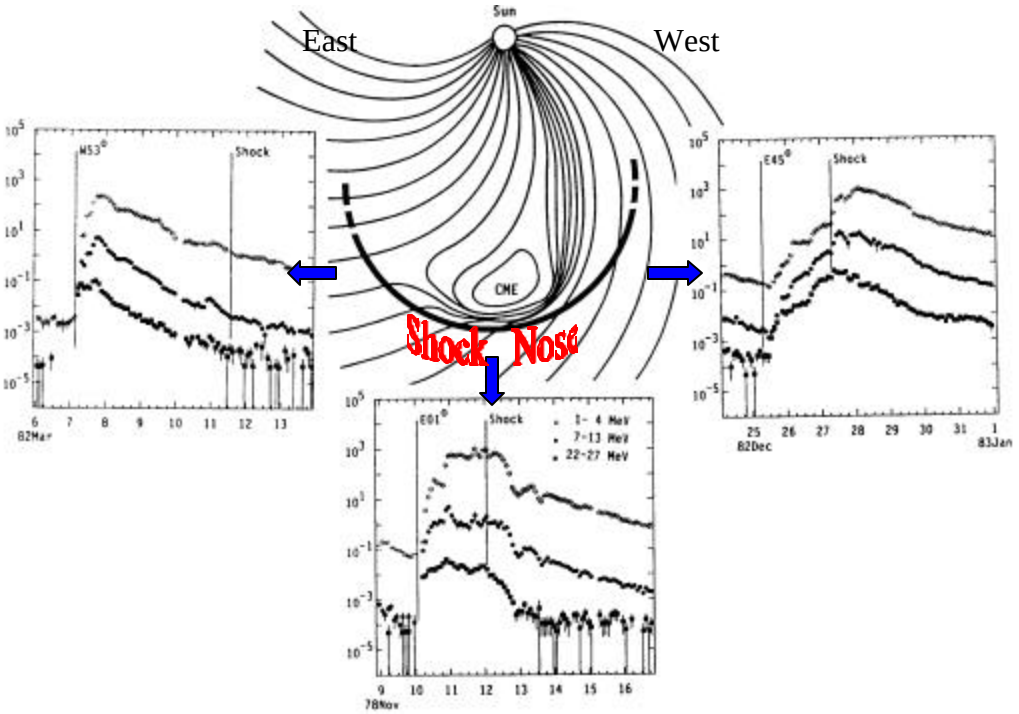

Figure 9. Intensity-time profiles for protons are shown for observers viewing a CME from three different longitudes [3, 34].

An observer on the east flank of the shock, as shown in Figure 9, sees a source at a western longitude on the Sun. As a function of time, this observer's connection point swings from the intense nose of the shock, near the Sun, to the weaker flank at 1 AU. In contrast, an observer on the west flank of the shock may see maximum intensity only after crossing through the shock into the region where field lines connect to the shock nose from behind. A sufficiently fast CME near central meridian will produce an intensity peak at the time of shock passage (seen in Figures 6 and 7, but not in Figure 9), followed by a sharp decrease in intensity when the observer enters the CME or magnetic cloud. The reduced intensity inside the CME shows that little or no acceleration occurs at reconnection regions or shock waves *behind* the CME. Occasionally, however, new events at the Sun do fill this region in and behind the CME with energetic particles (Kahler and Reames [15]).

The intensity-time profiles shown in Figure 9 are "typical" profiles obtained by observing hundreds of SEP events in different longitude intervals. However, on several occasions, it has been possible to measure the longitude distribution of SEPs around a single CME using multiple spacecraft. Figures 10 and 11 show two examples of individual events seen from different longitudes by 3 spacecraft (Reames, Kahler, and Ng [36]).

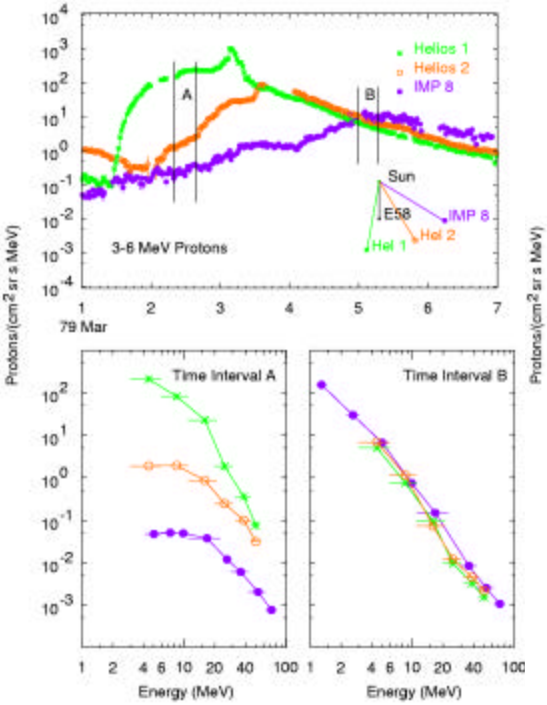

Figure 10. Proton intensities and spectra observed by 3 spacecraft in the 1979 March 1 event [36].

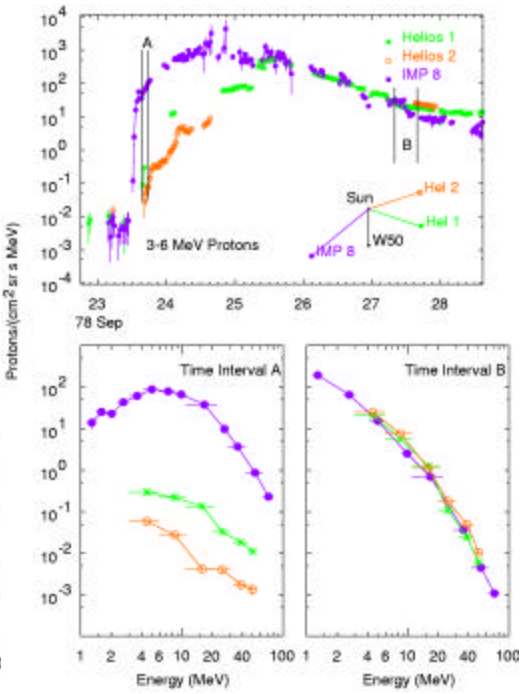

Figure 11. Proton intensities and spectra observed by 3 spacecraft in the 1978 September 23 event [36].

The insets in Figures 10 and 11 show the spatial distribution of the 3 spacecraft relative to the CME, denoted by its source longitude as seen from Earth. The CME is coming down in these insets just as it was in Figure 9.

In Figure 10, Helios 1 observes a source near central meridian so the proton intensity rises to a plateau value (near the streaming limit, described below), then it peaks at the time of shock passage, and subsequently declines. Helios 2 and IMP 8, on the west flank of the shock, see an event that rises less and less rapidly. The strong decline in intensity with longitude suggests a CME with a relatively narrow longitude span. However, intensities of all 3 spacecraft eventually converge to the same intensity that declines slowly with time. This is the "invariant spectral region," where all intensities and spectra are the same over a large spatial region. In this region, particles are essentially trapped in a magnetic "bottle" defined by the CME, which slowly expands with time. Adiabatic deceleration in this expanding bottle preserves the spectral shape.

The event in Figure 11 is much larger and more intense and the 3 spacecraft span a much larger angle of nearly 160°. The shock from this CME is seen at all 3 spacecraft and the intensity at Helios 2 rises rather rapidly considering that the source is behind the east limb as viewed from Helios 2. An invariant spectral re-

gion is again seen late in the event, despite the huge longitude span of the 3 spacecraft.

In addition to the longitude dependence, the acceleration at a given point on the shock can decrease strongly because the shock weakens as it expands radially. This dependence can be especially strong at high energies. Only the strongest shocks near central meridian produce shock peaks above 100 MeV at 1 AU, as we have seen. Protons above ~1 GeV are only accelerated when shocks are relatively near the Sun [52].

Kahler [12] plotted intensities of 470 MeV to 21 GeV protons as a function of the height of the leading edge of the CME at the time of acceleration, correcting for the proton transport time from the Sun. Figure 12 shows this plot for three large events in 1989. This plot shows that, although acceleration can begin when the shock is relatively low in the corona, maximum intensity of the high-energy protons occurs when the shock is in the region of ~5 to 10 solar radii.

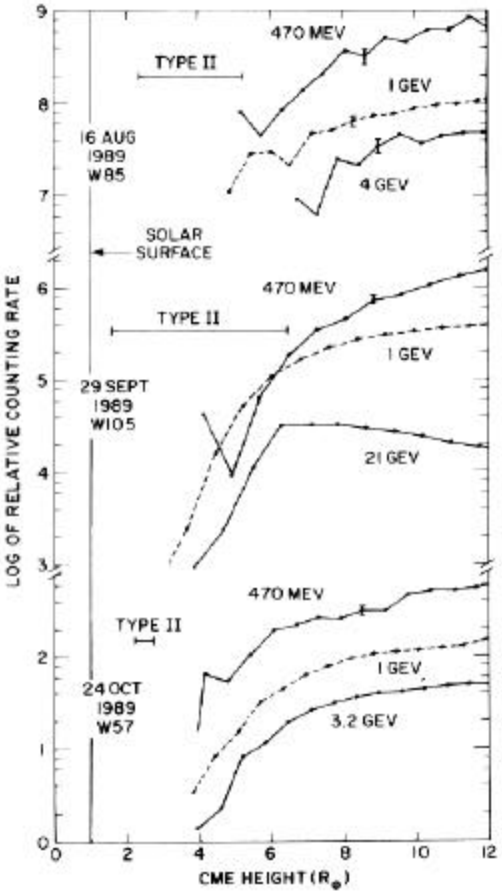

Figure 12. Proton fluxes are shown as a function of the CME height at the time of acceleration (after Kahler [12]).

The intensities of particles that are accelerated near the Sun decrease with distance approximately as R^{-3} as they expand outward in the diverging magnetic field. The fluence of particles from an event decreases approximately as R^{-2}, since event duration increases roughly as R.

3.3 The Streaming Limit

Since we know that shocks weaken as they move out toward 1AU and the particle spectra at the shock steepen, it seems quite surprising that the peak intensities occur late in events, when the shock is near 1 AU, and not early in the event when the shock is near the Sun and is much stronger.

In fact, the intensities that are seen early in an event are bounded at a value we call the "streaming limit." As particles stream away from a shock near the Sun, they generate Alfvén waves, as we described in Section 3.1. For a given energy, the intensities of both particles and resonant waves are in equilibrium and both decrease with distance from the shock. However, if we are able to increase the parti-

cle intensity at the shock, the new particles immediately increase the streaming and rapidly generate more resonant waves; these waves scatter the particles and reduce the streaming. The result is that the spatial gradient of particles and waves becomes steeper near the shock with little or no increase in the intensity at 1 AU. Figure 13 shows the streaming limits at three proton energies observed by Reames and Ng [38]. The value of the streaming limit in the region of a few MeV was established theoretically by Ng and Reames [29]. The observed value can vary by a factor of order 2 depending upon conditions near the shock. Once the shock arrives at 1 AU the full peak intensity that then exists at the shock is seen.

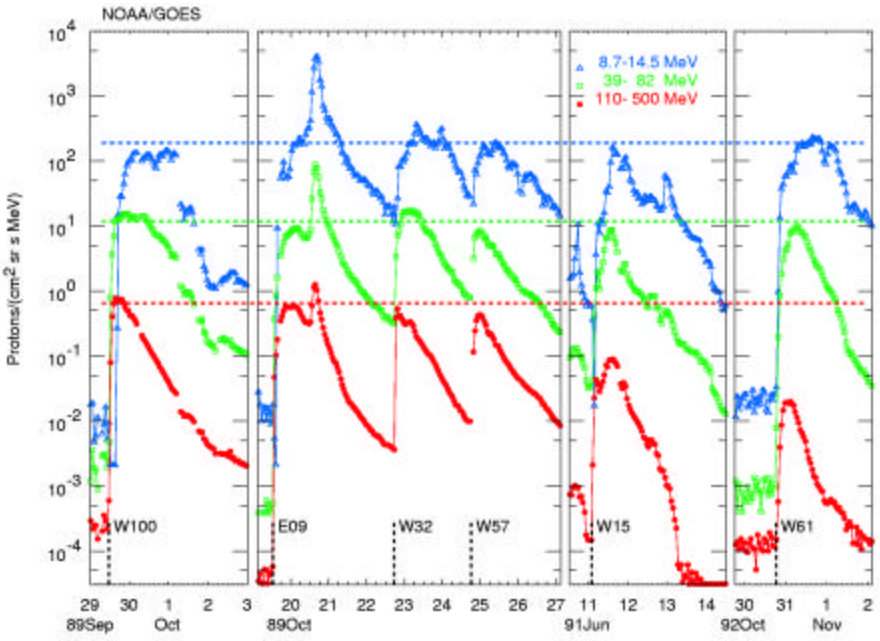

Figure 13. Intensity-time profiles are shown for six large events in three energy intervals. Early in the events, the intensities do not rise above the respective streaming limits, indicated by the dashed lines. Only the shock peaks on 1989 October 20 exceed these limits. [38]

3.4 Element Abundances and their Variations

For many years it has been clear that abundances of elements, averaged over many large gradual SEP events, were related to abundances of the solar corona (*e.g.* Meyer [25]). These coronal abundances differ from the corresponding abundances in the solar photosphere in a simple manner that depends upon the first ionization potential (FIP) of the element. A version of the "FIP-effect" based upon recent observations [34] is shown in Figure 14.

Since the elements with Z>2 in the corona and in SEP events are never singly ionized, the *first* ionization potential cannot possibly play a role in particle acceleration; the FIP-effect must already exist in the coronal material prior to acceleration. A similar FIP-effect is seen in comparing abundances in the solar wind or in direct coronal observations with those in the photosphere. The FIP effect is believed to occur as atoms are transported from the photosphere up into the corona along electric and magnetic fields. Low-FIP atoms are singly ionized in the corona while high-FIP atoms are neutral and can cross electromagnetic fields to return to the photosphere.

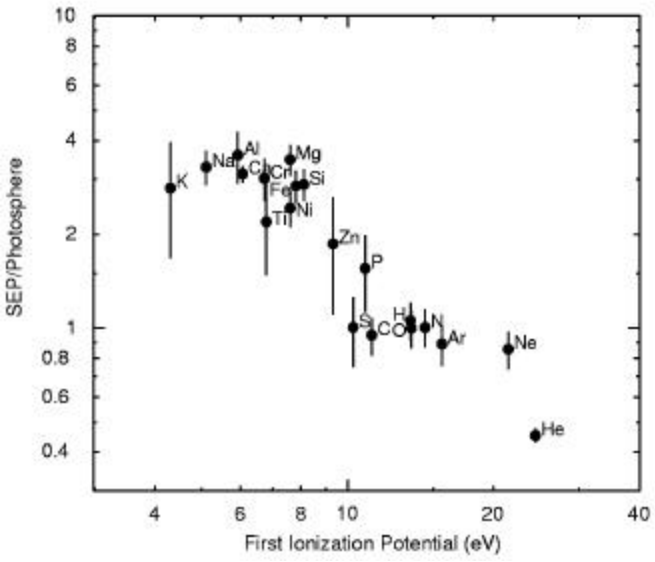

Figure 14. Average gradual-SEP element abundances relative to the photosphere are shown as a function of FIP. [34]

While the average abundances of gradual SEPs are independent of acceleration and transport of the particles, there are certainly substantial abundance variations from one event to another and variations with time during an individual event. These abundance variations depend upon the charge-to-mass ratio *Q/A* of the ions. Since abundance ratios are measured at a fixed velocity or energy/nucleon, ions with the same value of *Q/A* are affected in the same way by electromagnetic fields; hence, their ratios cannot vary. For heavy elements, Breneman and Stone [2] found that abundances in some events had a power-law dependence on *Q/A* with positive powers in some events and negative powers in others. However, this power-law dependence does on hold well in all events and does not extend to H at *Q/A*=1 (see Figure 3.8 in Reames [34]).

Abundances of different species are compared at the same energy/nucleon, *i. e.* at the same velocity. The acceleration and the transport time depend primarily on velocity. However, different species are scattered by proton-generated Alfvén waves with wave vector $k=B/mP$, where P is the particle rigidity. Therefore, different species in an abundance ratio, such as He/H or Fe/O, interact with different parts of the wave spectrum, depending on their values of *Q/A*. For example, for He/H at 2 MeV/amu, the H with *Q/A*=1 will resonate with waves produced by 2 MeV protons but the He, with *Q/A*=0.5 will resonant with waves produced protons of twice the velocity or 4 times the energy (non-relativistically), *i. e.* 8 MeV protons. Similarly, at 2 MeV/amu O^{+6} will resonate with waves produced by 14 MeV protons while Fe^{+14} resonates with waves produced by 32 MeV protons. Thus,

abundance ratios can explore the spectrum of ambient or proton-generated waves as the ions propagate out from the source. In intense SEP events, the intensities of both protons and resonant waves vary with space and time; element abundances can probe these variations in the wave spectrum.

Figure 15 shows the regular time-dependent variation of element abundances in a large SEP event (see Tylka *et al.* [51]) and compares them with abundances derived from a theoretical simulation of the evolution of the particle and wave spectra in space and time during the event (see Ng *et al.* [30]).

One might expect that the first particles to arrive from an SEP event would traverse an ambient Kolmogorov wave spectrum and a scattering mean free path $\lambda \sim P^{1/3}$. Such a spectrum would scatter Fe less than O and He less than H, so that Fe/O and He/H would begin at high values and decline with time. Figure 16 shows that this initial behavior does occur in the 2000 April 4 event, but in the 1998 September 30 event, He/H begins at a low value and rises initially (Reames, Ng, and Tylka [41]).

The reason for the rising He/H ratio in the 1998 September 30 event is that the 2 MeV/amu He resonates with

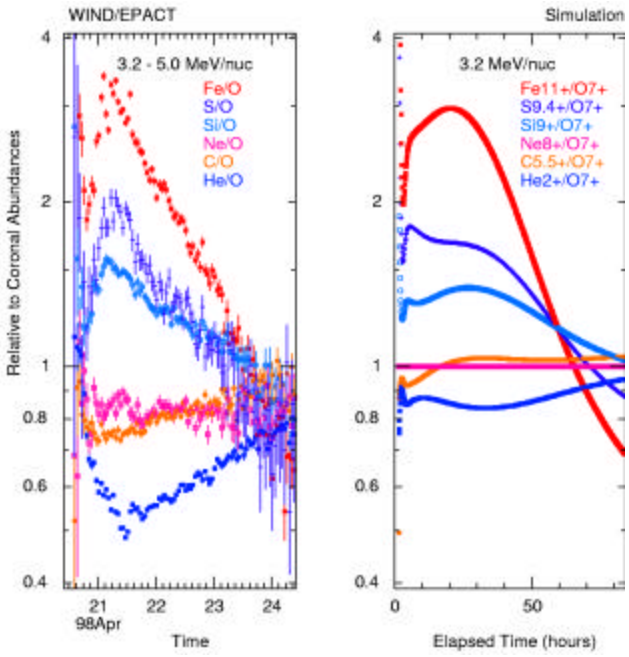

Figure 15. A comparison of observations and theory shows the time variations of abundance ratios as elements propagate through proton-generated Alfvén waves.

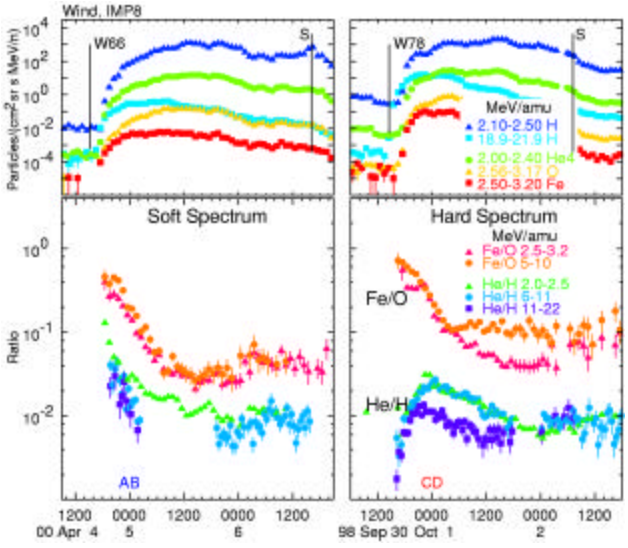

Figure 16 The two events show similar behavior of Fe/O but different behavior of He/H because of the increased wave generation by high-energy protons in the 1998 September 30 event (see Reames, Ng, and Tylka [41]).

waves generated by ~8 MeV H that arrived much earlier than the 2 MeV H. Thus the 2 MeV/amu He is scattered more than the 2 MeV H and arrives later. The intensity of ~5-20 MeV protons is over an order of magnitude higher in the 1998 September 30 event than it is in the 2000 April 4 event. This higher level of wave generation is adequate to reverse the behavior of He/H in the September event.

3.5 Energy Spectra

Energy spectra generated by a shock at equilibrium are power-law in form; the spectral power is related to the shock compression ratio (see Jones and Ellison [8]). The spectrum observed at a distance from the shock is then modified by transport as described above. At high energies, however, the shock spectrum may be modified because of decreased wave generation, the finite acceleration time, or spatial effects that cause high-energy particles to leak away from the shock. This leakage causes an exponential rollover of the spectra to produce a form $E^{-g}\exp(-E/E_{knee})$ (see Ellison and Ramaty [5]).

Figure 17 shows spectra for which the e-folding or "knee" energies for protons differ by a factor of over 60. Below about 10 MeV, the intensities and spectra are similar for the two events shown; the low-energy protons are not a predictor of the high-energy behavior. Factors that control the knee energy are not well understood. This is a particular problem for predicting the radiation hazard to astronauts and equipment in space since shielding against protons >100 MeV is very difficult.

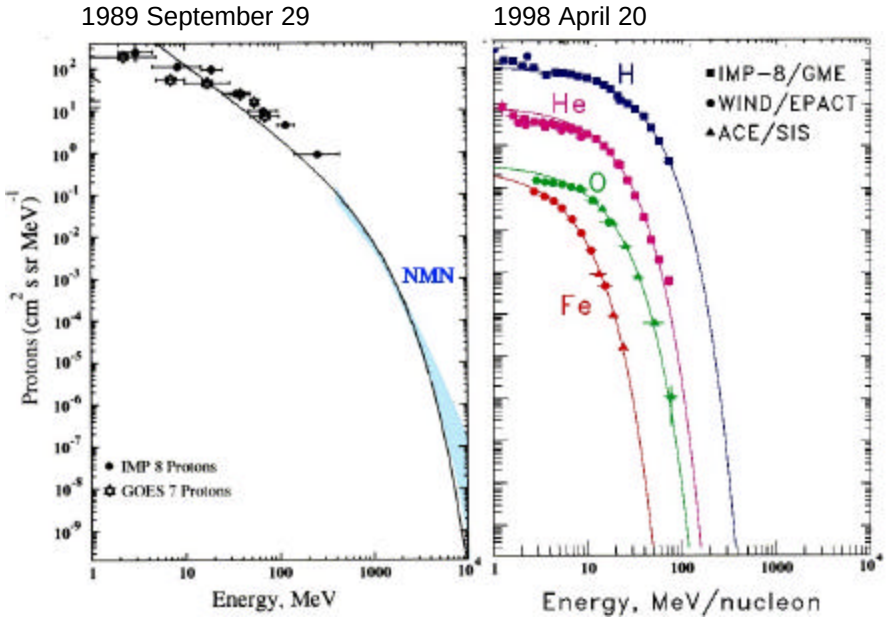

Figure 17. Spectra in two events are fit to the form $E^{-g}\exp(-E/E_{knee})$ (Ellison and Ramaty [5]). In the 1989 September 29 event (Lovell *et al.* [21]) the knee energy of ~1 GeV falls in the region measured by the ground-level neutron monitor network (NMN). In the 1998 April 20 event (Tylka *et al.* [49]) the proton knee is at 15 MeV; for other species, E_{knee} scales as Q/A.

Variation in the knee energy for different ion species can also be seen in Figure 17 for the 1998 April 20 event. For many, but not all, events, E_{knee} varies as Q/A (Tylka *et al*. [49]). In such events, this dependence may be used to determine the ionization states of elements up to Z~40 (Reames *et al.* [42]) and to detect the presence of a small admixture of residual suprathermal ions from previous impulsive flares that have been accelerated by the shock (Tylka *et al.* [50]).

3.6 Angular Distributions

Transport of SEPs along the local magnetic field can be studied by observing angular distributions of the ions and their variation with time. Figure 18 shows angular distributions, relative to the direction of the magnetic field, for He in two energy intervals and for O and Fe. These angular distributions, projected in the ecliptic plane, were measured aboard the Wind spacecraft with its spin axis orthogonal to the ecliptic (see Reames, Ng, and Berdichevsky [39]).

The conditions of the interplanetary medium during the SEP events of May 2 and May 6 (shown in Figure 18) were quite unusual since each of these events began when the Earth was immersed in the large magnetic cloud associated with a previous CME. In these large clouds, the magnetic energy density greatly dominates the thermal energy in the solar wind plasma, so the magnetic fields are regular and undisturbed. Thus, the particles stream easily along the magnetic field with minimum pitch-angle scattering for periods as long as a day.

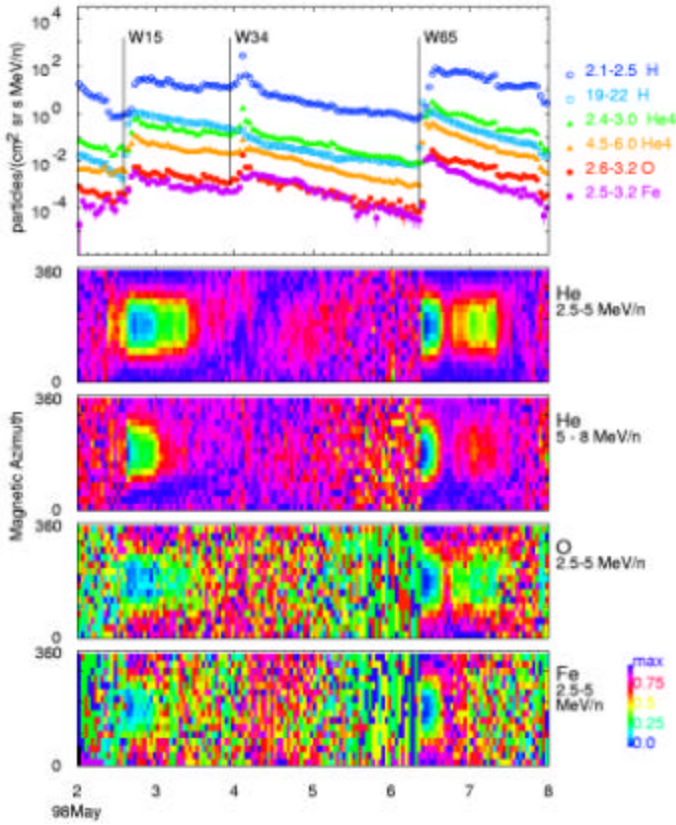

Figure 18. Angular distributions of ions relative to the direction of the magnetic field are shown for He (2 energies), O, and Fe in SEP events during 1998 May. [39]

The ratio of the thermal and magnetic energy is defined by the plasma β, so that $\beta = nkT / (B^2/8\pi)$. For the energetic ions, we define the front-to-back ratio, F/B, as the

number of ions flowing outward in a 45° interval centered on the field direction divided by the number flowing inward in a 45° interval in the opposite direction. These quantities along with other plasma parameters are shown in Figure 19 for the same period in 1998 May.

Figure 19 shows that *F/B* reaches values above 10 for several hours, and that values above 2 persist for more than a day during both of the events in 1998 May. This unusually strong streaming occurs during periods of unusually low b and, in fact, *F*/*B* decreases when b increases.

The events on May 2 and 6 are associated with CMEs with speeds of ~1000 km/s, and are not extremely large. A slower CME late on May 3 (W34) produces no intensity increase. However, a sharp peak is seen at the strong shock early on May 4.

Very large SEP events appear capable of enough wave generation, even at 1 AU, to stop this kind of strong persistent streaming. However, correlation of streaming with b is also seen in these events (see Reames, Ng, and Berdichevsky [39]).

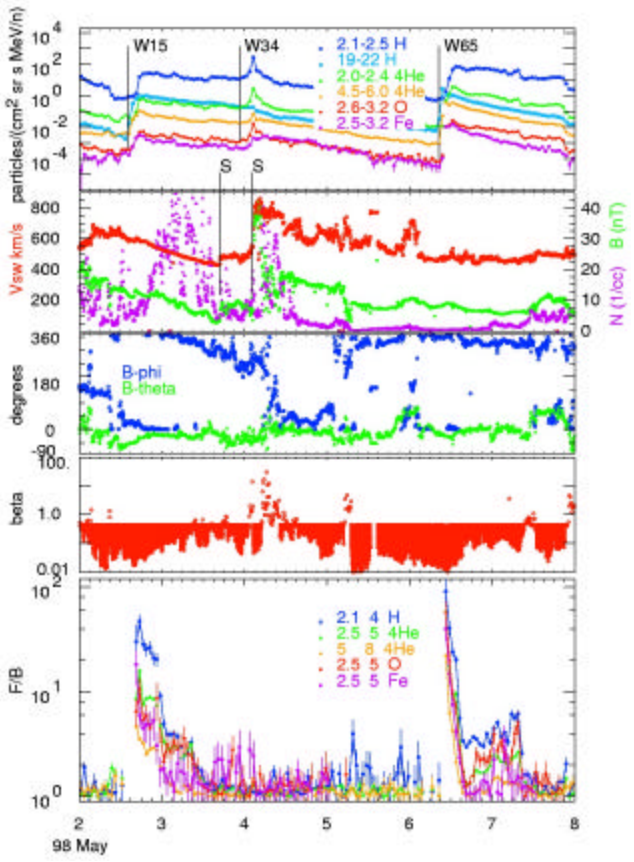

Figure 19. Various plasma parameters and the front/back ratio for ions are shown for the 1998 May period seen in Figure 18. [39]

4. Magnetic Topology of Flares, CMEs, and Particle Acceleration

Gamma-ray lines are produced when flare-accelerated particles plunge into the solar atmosphere. Narrow gamma-ray lines of C, O, or Fe, for example, are produced in nuclear reactions when ambient ions are excited by accelerated protons. Broad gamma-ray lines are the result of Doppler-shifted lines emitted from ions of the "beam" that have interacted with atmospheric protons. Element abundances for both ambient and accelerated elements may be derived from the line strengths of the narrow and broad lines, respectively. Narrow lines show the same coronal

abundances that we find in gradual SEP events (Ramaty *et al.* [31]). However, the broad lines show that the "beam" is ^{3}He-rich (Mandzhavidze, Ramaty, and Kozlovsky [23]) and Fe-rich (Murphy *et al.* [28]) just like impulsive SEP events. Since the broad- and narrow-line abundances are different, the enhancements must be the produced during acceleration.

Thus, in the large events with both flares and CMEs, we see impulsive-flare abundances in the broad gamma-ray lines but not in the SEPs out in space. We only see impulsive SEPs from small flares. We can resolve this apparent paradox by considering the probable magnetic topology of the different events.

Figure 20 shows the magnetic topology on the Sun produced by emerging flux of opposite polarity to that of the overlying field. This reconnection region (red) is rich in wave turbulence that can result in resonant stochastic acceleration of both electrons (Miller, LaRosa, and Moore [26]) and ions (Temerin and Roth [46]; Miller and Reames [27]; Roth and Temerin [44]; Litvinenko [20]) with the unusual abundances that are observed. The accelerated particles have easy access to open magnetic fields that they can follow out to Earth.

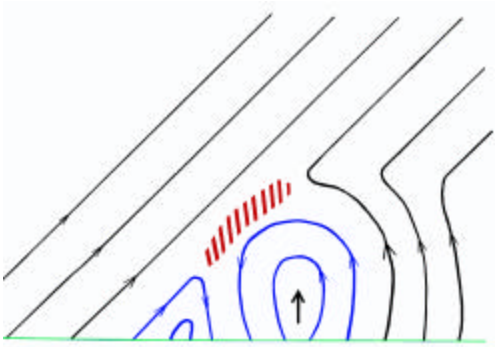

Figure 20. The magnetic topology leading to an impulsive SEP event involves magnetic reconnection (red) at open field lines (black).

The model in Figure 20 was proposed by Shimojo and Shibata [45] to describe X-ray jets and the source of the 10-100 keV electrons that produce interplanetary type III radio bursts (Robinson and Benz [43]). The model was also considered by Kahler *et al.* [16] for impulsive SEP events with narrow CMEs. Hot plasma that is ejected on the open field lines is confined to a narrow region of magnetic flux tubes connected to the source.

Large gradual SEP events have a completely different topology shown in Figure 21 (see Forbes [7]). Here the reconnection region (red) is deep within closed magnetic fields. Particles accelerated in this region are also ^{3}He-rich and Fe-rich, according to the gamma-ray

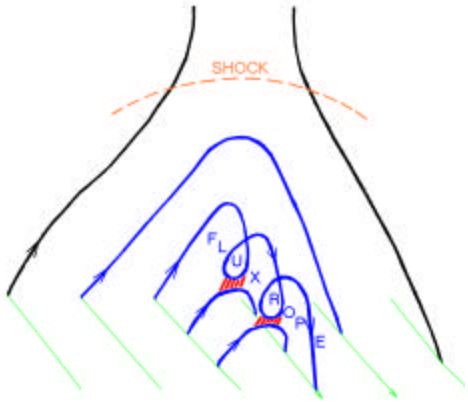

Figure 21. The magnetic topology leading to a gradual SEP event involves reconnection (red) deep within closed fields (blue) and ejection of a fast CME that drives a shock.

measurements, but they are trapped and cannot escape; eventually they scatter into the loss cone and plunge into the solar atmosphere at the foot points of the magnetic field lines on a time scale of hours. None of these particles remains inside the CME when it arrives near Earth. For those events in which the CME drives a sufficiently fast shock, particles are accelerated by the shock on open field lines. The shock normally accelerates suprathermal ions from the ambient plasma of the corona and solar wind. However, since shocks can accelerate any suprathermal ions they encounter, residual ions from previous impulsive and gradual events may be included.

Finally, we should point out that the interplanetary magnetic topology can become quite complex. During solar maximum, CMEs are ejected from the Sun at a sufficient rate to produce an average of one CME per AU per steradian. Less than 5% of these CMEs are fast enough to produce SEP events, many contain strong magnetic clouds, but most produce leaky magnetic bottles that tend to trap SEPs. Such conditions affect particle streaming-anisotropies or produce invariant spectra. Furthermore, fast CMEs can also overtake slower ones causing highly variable acceleration conditions at the shock (Gopalswamy et al. [9]).

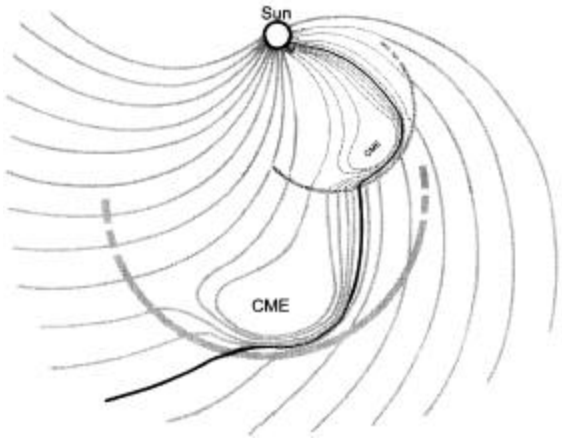

Figure 22. Multiple CMEs can affect particle streaming and produce magnetic bottles even when they are not fast enough to accelerate particles.

REFERENCES

[1] Bell, A. R.: 1978, *Mon. Not. Roy. Astron. Soc.*, **182**, 147.

[2] Breneman, H. H., and Stone, E. C. 1985, *Astrophys. J. (Letters)* **299**, L57.

[3] Cane, H. V., Reames, D. V., and von Rosenvinge, T. T. 1988, J. Geophys. Res. 93, 9555.

[4] Desai, M. I., Mason, G. M., Dwyer, J. R., Mazur, J. E., Smith, C. W., and Skoug, R. M. 2001, *Astrophys. J. (Letters)* **553**, L89

[5] Ellison, D., and Ramaty, R. 1995, *Astrophys. J.* **298**, 400.

[6] Fisk, L. A. 1978 *Astrophys. J.* **224**, 1048.

[7] Forbes, T. G. 2000, *J. Geophys. Res.* **105**, 23153.

[8] Jones, F. C., and Ellison, D. E. 1991, *Space Sci. Revs.* **58**, 259.

[9] Gopalswamy, N., Yashiro, S., Kaiser, M. L., Howard, R. A., Bougeret, J.-L. 2001, *Astrophys. J. (Letters)* **548**, L91.

[10] Gosling, J. T. 1993, *J. Geophys. Res.*, **98**, 18949.

[11] Kahler, S. W. 1992, *Ann. Rev. Astron. Astrophys*. **30**, 113.

[12] Kahler, S. W. 1994, *Astrophys. J*. **428**, 837.

[13] Kahler, S. W. 2001, *J. Geophys. Res.* **106**, 20947.

[14] Kahler, S. W., Cliver, E. W., Cane, H. V., McGuire, R. E., Stone, R. G. and Sheeley, N. R., Jr. 1986, *Astrophys. J*. **302**, 504.

[15] Kahler, S. W. and Reames, D. V. 1991, *J. Geophys. Res.* **96**, 9419.

[16] Kahler, S. W., Reames, D. V., and Sheeley, N. R., Jr. 2001, *Astrophys. J.* **562**, 558.

[17] Kahler, S. W., Sheeley, N. R. Jr., Howard, R. A., Koomen, M. J., Michels, D. J., McGuire, R. E., von Rosenvinge, T. T. and Reames, D. V. 1984, *J. Geophys. Res.* **89**, 9683.

[18] Lee, M. A. 1983, *J. Geophys. Res.* **88**, 6109.

[19] Lee, M. A. 1997, in: *Coronal Mass Ejections*, edited by N. Crooker, J. A. Jocelyn, J. Feynman, Geophys. Monograph 99, (AGU press) 227.

[20] Litvinenko, Y. E. 2001, in Solar and Galactic Composition, Ed. R. F. Wimmer-Schweingruber, *AIP Conf. Proc*. **598**, p. 311.

[21] Lovell, J. L., Duldig, M. L., Humble, J. E. 1998, *J. Geophys. Res.* **103**, 23,733.

[22] Luhn, A., Klecker, B., Hovestadt, D., and Möbius, E. 1987, *Astrophys. J*. **317**, 951.

[23] Mandzhavidze, N., Ramaty, R., and Kozlovsky, B. 1999, *Astrophys. J*. **518**, 918.

[24] Mason, G. M., Mazur, J. E., and Dwyer, J. R. 1999, *Astrophys. J. (Letters)* **525**, L133.

[25] Meyer, J. P. 1985, *Astrophys. J. Suppl*. **57**, 151.

[26] Miller, J. A., LaRosa, T. N., and Moore, R. L. 1996, *Astrophys. J.* **461**, 445.

[27] Miller, J. A., and Reames, D. V., 1996, in High Energy Solar Physics, Eds. R. Ramaty, N. Mandzhavidze, X.-M. Hua, *AIP Conf. Proc.* **374**, p. 450.

[28] Murphy, R J., Ramaty, R., Kozlovsky, B., and Reames, D. V. 1991, *Astrophys. J*. **371**, 793.

[29] Ng, C. K., and Reames, D. V. 1994 *Astrophys. J*. **424**, 1032.

[30] Ng, C. K., Reames, D. V., and Tylka, A. J. 1999a, Geophys. Res. Lett. **26**, 2145.

[31] Ramaty, R., Mandzhavidze, N., and Kozlovsky, B. 1996, in High *Energy Solar Physics*, Eds. R. Ramaty, N. Mandzhavidze, X.-M. Hua, *AIP Conf. Proc*. **374**, p. 172.

[32] Reames, D. V., 1990, *Astrophys. J. Suppl*. **73**, 235.

[33] Reames, D. V. 1995, *Revs. Geophys. (Suppl.)* **33**, 585.

[34] Reames, D. V. 1999, *Space Sci. Revs*. **90**, 413.

[35] Reames, D. V. 2000, *Astrophys. J. (Letters)* **540**, L111.

[36] Reames, D. V., Kahler, S. W., and Ng, C. K. 1997, *Astrophys. J.* **491**, 414.

[37] Reames, D. V., Meyer, J. P., and von Rosenvinge, T. T. 1994, *Astrophys. J. Suppl.* **90**, 649.

[38] Reames, D. V. and Ng, C. K. 1998, *Astrophys. J.* **504**, 1002.

[39] Reames, D. V., Ng, C. K., and Berdichevsky, D. 2001, *Astrophys. J.* **550**, 1064.

[40] Reames, D. V., Ng, C. K., and Tylka, A. J. 1999, *Geophys. Res. Lett.*, **26**, 3585.

[41] Reames, D. V., Ng, C. K., and Tylka, A. J. 2000, *Astrophys. J. (Letters)* **531**, L83.

[42] Reames, D. V., Ng, C. K., and Tylka, A. J. 2001, *Astrophys. J. (Letters)* **548**, L233.

[43] Robinson, P. A. and Benz, A. O. 1998, *Sol. Phys.* **194**, 345.

[44] Roth, I., and Temerin, M. 1997, *Astrophys. J.* **477**, 940.

[45] Shimojo, M., and Shibata, K. 2000, *Astrophys. J.* **542**, 1100.

[46] Temerin, M., and Roth, I. 1992, *Astrophys. J. (Letters)* **391**, L105.

[47] Tylka, A. J. 2001, *J. Geophys. Res.* **106**, 25333.

[48] Tylka, A. J., Boberg, P. R., Adams, J. H., Jr., Beahm, L. P., Dietrich, W. F., and Kleis, T. 1995, *Astrophys. J.* (*Letters*) **444**, L109.

[49] Tylka, A. J., Boberg, P. R., McGuire, R. E., Ng, C. K., and Reames, D. V. 2000, in *Acceleration and Transport of Energetic Particles Observed in the Heliosphere*, eds. R.A. Mewaldt, J.R. Jokipii, M.A. Lee, E. Moebius, and T.H. Zurbuchen, *AIP Conf. Proc.* **528**, p 147.

[50] Tylka, A. J., Cohen, C. M. S., Deitrich, W. F., Maclennan, C. G., McGuire, R. E., Ng, C. K., and Reames, D. V. 2001, *Astrophys. J. (Letters)* **558**, L59,

[51] Tylka, A. J., Reames, D. V., and Ng, C. K. 1999, *Geophys. Res. Lett.* **26**, 2141.

[52] Zank, G. P., Rice, W. K. M., Wu, C. C. 2000, *J. Geophys. Res.* **105**, 25079.